

# *In situ* cell for grazing-incidence x-ray diffraction on thin films in thermal catalysis

Cite as: Rev. Sci. Instrum. 95, 033904 (2024); doi: 10.1063/5.0179989

Submitted: 6 October 2023 • Accepted: 17 February 2024 •

Published Online: 6 March 2024



View Online



Export Citation



CrossMark

Lukas Thum,<sup>1,a)</sup> Manuela Arztmann,<sup>1</sup> Ivo Zizak,<sup>1</sup> René Grüneberger,<sup>1</sup> Alexander Steigert,<sup>1</sup>   
Nico Grimm,<sup>1</sup> Dirk Wallacher,<sup>1</sup> Rutger Schlatmann,<sup>1,2</sup> Daniel Amkreutz,<sup>1</sup> and Albert Gili<sup>1</sup>

## AFFILIATIONS

<sup>1</sup> Helmholtz-Zentrum Berlin für Materialien und Energie, 14109 Berlin, Germany

<sup>2</sup> HTW Berlin–University of Applied Sciences, 12459 Berlin, Germany

<sup>a)</sup> Author to whom correspondence should be addressed: [lukas.thum@helmholtz-berlin.de](mailto:lukas.thum@helmholtz-berlin.de)

## ABSTRACT

A cell for synchrotron-based grazing-incidence x-ray diffraction at ambient pressures and moderate temperatures in a controlled gas atmosphere is presented. The cell is suited for the *in situ* study of thin film samples under catalytically relevant conditions. To some extent, in addition to diffraction, the cell can be simultaneously applied for x-ray reflectometry and fluorescence studies. Different domes enclosing the sample have been studied and selected to ensure minimum contribution to the diffraction patterns. The applicability of the cell is demonstrated using synchrotron radiation by monitoring structural changes of a 3 nm Pd thin film upon interaction with gas-phase hydrogen and during acetylene semihydrogenation at 150 °C. The cell allows investigation of very thin films under catalytically relevant conditions.

© 2024 Author(s). All article content, except where otherwise noted, is licensed under a Creative Commons Attribution (CC BY) license (<http://creativecommons.org/licenses/by/4.0/>). <https://doi.org/10.1063/5.0179989>

## INTRODUCTION

Since the early stages of catalysis research, thin films and single crystals are of interest as model systems for understanding catalytic processes on surfaces.<sup>1–3</sup> With the developments in microelectronics allowing precise control and reproducibility of sub-nanometer thin structures as well as advances in photovoltaics and display technologies that allow large-scale processing of such films with tailored electronic properties, thin films can still help understand complex catalytic processes and potentially tailor the functionality of heterogeneous catalysts and even their upscaling to industrially relevant quantities. The key to understanding the functionality of catalysts are *in situ* and operando studies.<sup>4–6</sup>

The proficiency of a material to function as a catalyst has been traditionally considered to be correlated with its surface properties. More recently, the subsurface chemistry of a catalyst has also been determined to play a crucial role in the dry reforming of methane<sup>7</sup> and in acetylene semihydrogenation.<sup>8,9</sup> XRD is a bulk sensitive technique, capable of unraveling the formation of metastable phases under reaction conditions necessary to understand the nature of the active catalyst but elusive to *ex situ* studies.<sup>10</sup> Compared to other x-ray techniques, such as X-ray Photoelectron Spectroscopy (XPS)

or X-ray Absorption Spectroscopy (XAS) of lighter elements or outer shells requiring the use of low photon energies, XRD can make use of hard monochromatic x rays, allowing easier penetration of the reactor walls and being unaffected by the gas atmosphere, thereby minimizing the pressure gap and making the measuring conditions comparable to real-world applications.<sup>11</sup>

In contrast to Bragg–Brentano and transmission XRD, which is commonly employed in catalytic operando studies,<sup>12–14</sup> grazing incidence x-ray diffraction GIXRD [or grazing-incidence wide-angle x-ray scattering (GIWAXS)] offers a high surface sensitivity, which is most relevant for catalytic studies.<sup>15</sup>

Especially in electrochemistry, GIXRD is an obvious choice and often deployed for operando studies.<sup>16–18</sup> However, in thermal catalysis this technique is usually only applied in operando studies on model systems<sup>19,20</sup> due to the requirements to the sample not being compatible with the commonly used powder catalyst. For electrochemical GIXRD cells, the windows are often made from Kapton<sup>®</sup> as it is rather inert, thermally stable at temperatures above 200 °C, and resistant to many electrolytes. Additionally, for these applications, the cell's body needs to be electrically insulating, thus limiting the choice of materials. Usually, chemical-resistant machinable polymers are used to manufacture such cells. With those usually being

thermally insulating and having rather limited operating temperatures, these materials are not desirable in thermal catalysis. There are cells reported and also commercially available allowing GIXRD to be performed in controlled gas atmospheres and at high temperatures using, for example, beryllium windows,<sup>21–25</sup> but due to their dome-like structure, although optimized for XRD measurements, their application under continuous gas flow and/or the need for swift gas change responses is limited. Although there are designs that are already considering reducing the total gas volume<sup>25</sup> with about 50 ml reactor volume, gas diffusion rates might dominate the measured kinetics. In particular, commercial cells are often constructed of metals using inlaying thermocouples and heating wires, rendering them non-resistant to gases such as hydrogen or carbon monoxide in high concentrations and, even worse, being not inert in a lot of catalytic applications. To overcome these issues, home-built systems are being deployed.<sup>26</sup> A synchrotron environment combined with a 2D detector has several advantages compared to a typical lab-based source and 0D or 1D detectors with the most obvious being the high photon flux, strongly reducing the integration times and allowing time-sensitive measurements. Furthermore, the 2D detector allows simultaneous measurement of diffraction (or scattering) and reflectivity, providing information on the film's thickness, in-plane crystal orientation (also called texture), density, and roughness.

In this work, a GIXRD cell is presented, allowing *in situ* studies of thin, catalytically active films in the thickness range down to several nanometers in catalytic applications using synchrotron x-rays. The cell design is presented; different domes to enclose the sample are tested and their influence in the diffraction patterns quantified; the capacity of the cell to provide simultaneous information of XRF and XRR is discussed; and finally, the time and thickness resolution of the cell in the  $\mu$ -Spot beamline of the BESSY-II synchrotron is demonstrated.

## CELL DESIGN

The design is focused on GIXRD measurements, using very shallow incidence angles of the x-ray beam, resulting in a maximized surface sensitivity. Although the main foci of this design are the XRD studies conducted using a 2D static detector, small and wide-angle scattering, reflectivity, and, to a certain degree, x-ray fluorescence (XRF) can also be performed in this cell simultaneously.

The reaction cell (Figs. 1, S1, and S2) consists of a CNC milled heating body (10) made of brass, powered by heating cartridges (14), and controlled via a Pt100 (class A) plus a redundant K-type thermocouple inside the brass body. Brass as the body material was chosen because it is easily machined and has a high thermal conductivity, ensuring a homogeneous temperature distribution in the cell. To improve the chemical resistance and prevent the brass to partake in the chemical reaction, the cell was electroplated with gold, which can be considered inert in most chemical applications. An aluminum lid (8) with an x-ray transparent Kapton<sup>®</sup> (9, polyimide, 50  $\mu$ m thickness) window forms a 1.3 mm wide gas channel above the sample (12). The brass body is equipped with two 1/16 in. (11) connections for the gas inlet and outlet (13). In the front and back of the sample pocket, the brass is milled down to ensure that the x rays do not interact with the brass body even at very low incidence angles. Using polyimide, the current maximum operating temperature is limited to about 250 °C. To increase the temperature limit in the

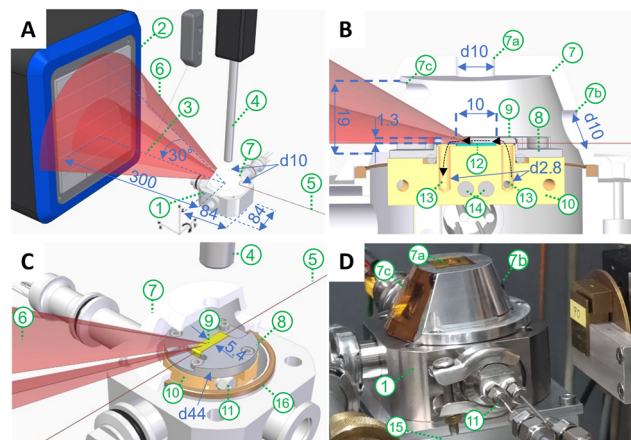


**FIG. 1.** (a) Sketch of the beam path. The red cones indicate diffraction at 20° and 30°. A beamstop is positioned to block the primary x-ray beam and protect the detector; (b) cross section of the *in situ* cell; (c) partial cut of the home-built *in situ* cell; (d) photograph of the cell in the beamline with 1: GIXRD cell, 2: 2D x-ray detector, 3: beamstop, 4: fluorescence detector, 5: incident beam, 6: diffracted beam, 7: outer dome with openings for fluorescence (a), incident beam (b), and diffraction (c), 8: aluminum cap, 9: 50  $\mu$ m Kapton<sup>®</sup> window, 10: gold plated brass body, 11: gas connections, 12: sample, 13: gas inlet/outlet, 14: heating cartridges, 15: translation stage, 16: dome sealing, 17: cell sealing, and 18: ceramic stilt. The dimensions are provided in mm.

future, a full ceramic/glass version is under development. In contrast to common commercial designs, no heating wire or thermocouple is in direct contact with the gas-phase in this design. This is crucial when working with high concentrations of hydrogen, oxygen, or carbon monoxide, which might react with the materials leading to embrittlement or taking part in the reaction, causing unwanted side reactions. Especially with the heating wires, side reactions are often unavoidable, which have the highest temperature in the system. The sample is mounted in a 700  $\mu$ m deep 10.2  $\times$  10.2 mm<sup>2</sup> pocket in the brass body and covered with the aluminum lid, exposing about 5 mm in width and 10 mm in length of the sample to the gas and the x rays (see Figs. S1 and S2). When using samples with accurate thicknesses, the lid helps press the sample into the pocket to straighten it and thus simplify the alignment in the x-ray beam. In its closed form, the Kapton<sup>®</sup> lid and sample form a channel with a width of about 1.3 mm for the gas to pass over the sample. The narrow channel with a low volume enables dynamic experiments, swiftly replacing the gas phase over the sample, thus allowing for the kinetic measurements of gas-sensitive phase transitions. The hydrodynamic residence time above the catalyst is at reasonable flow rates well below one second and can be even in the milliseconds at higher flow rates. Therefore, transient experiments will mostly be limited by the gas inlet/outlet and gas delivery system. Due to the geometry, the Reynolds numbers in this system are rather low, below 100 with the here mostly applied 40 Nml/min; therefore, a laminar flow profile is expected in the system. An even narrower channel to achieve a turbulent regime would be beneficial in this case for the gas–catalyst interaction and could help avoid the formation of a laminar flow profile in the system. Nevertheless, this option was disregarded as further narrowing the channel would mean the

Kapton window is within the beam spot along the path length, greatly increasing the background scattering intensity (see Fig. S1). The estimated  $Da_{II}$  for hydrogen in this cell indicates that especially at higher contact times, mass transport effects should be negligible (see the supplementary material, Fig. S12).<sup>27</sup> To ensure a good temperature homogeneity and reduce the heat loss by conduction, the *in situ* cell is mounted on ceramic stilts (18, supplementary material) inside the outer cell (1). The outer cell is operable in high vacuum for insulation, which further avoids temperature gradients. By monitoring the insulation vacuum pressure, leakage of the reactor cell can be easily detected. The vacuum chamber is closed by an x-ray transparent dome (7). For this part, a commercial graphite (graphite dome DHS, 250  $\mu\text{m}$ , Anton Paar), a commercial PEEK dome (polyether ether ketone PEEK dome DHS, 250  $\mu\text{m}$ , Anton Paar), and a home-built Kapton<sup>®</sup> dome (13  $\mu\text{m}$  thickness for the small windows 7a+b, and 50  $\mu\text{m}$  thickness for the big one 7c) were tested, with Kapton<sup>®</sup> not only being the best in terms of x-ray transmittance as later proven but also the least mechanically stable. While the PEEK and graphite materials can be manufactured in a spherical geometry to withstand the 1 bar pressure difference, thin Kapton<sup>®</sup> foil must be glued on a mechanically stable support. With their spherical geometry, the PEEK and graphite domes allow the full  $0^\circ$ – $180^\circ$  range for incidence and diffraction angles, whereas the Kapton<sup>®</sup> one, requiring a support, has some angular restrictions. Since the current cell was designed for deployment in the synchrotron environment using a 2D detector, an aluminum skeleton was designed using Kapton<sup>®</sup> windows for the incident beam (7b), the scattered x-rays in the angle range of  $0^\circ$ – $32^\circ$  (7c), and a window at  $90^\circ$  allowing simultaneous XRF measurements (7a). Using the double dome design also has safety advantages, especially in environments not equipped for the handling of hazardous gases. In the case of sealing failure or window rupture of the reactor, the escaping gases will be confined in the outer dome and, subsequently, be removed by the vacuum pump.

For temperature control, a Model 336 controller from Lake Shore Cryotronics Inc. (USA) was used. The gases were dosed using a home-built gas dosing system (Fig. S3) consisting of mass flow controllers (MFCs, El-Flow prestige series, Bronkhorst) for mixing up to three different gases and a back pressure regulator (El-Press series, Bronkhorst) to adjust the working pressure of the cell. Data logging and control of these devices were ensured by a customized LabVIEW program. For gas analysis, a mass spectrometer (Prisma 80, Pfeiffer) was connected to the exhaust. While closed, the operating pressure of the cell was kept at around 1.1 bars, while applying a total flow rate of about 40 Nml/min. For the lower temperature ( $<150^\circ\text{C}$ ) applications presented here, the pressure in the outer dome was usually held at just 0.2 bar below the cell pressure to avoid higher stresses on the Kapton<sup>®</sup> windows of the reactor lid.

## X-RAY MEASUREMENTS

X-ray measurements were conducted at the  $\mu$ -Spot beamline of the Bessy II synchrotron in Berlin, Germany.<sup>28,29</sup> The incident beam (5) was adjusted to 17 keV photon energy (corresponding to a wavelength of 0.7293  $\text{\AA}$ ) with a spot size of 30  $\mu\text{m}$  in diameter. A Dectris Eiger 9M detector (2) was used at a distance of about 300 mm from the sample. The correct values for the sample to detector distance (SDD) were calibrated using a LaB<sub>6</sub> NIST 660b standard sample. This was prepared by coating the standard on a Si-wafer of the same dimensions as the catalyst samples. The samples were loaded in the home-built cell (Fig. 1, 1) mounted on an XY stage, a goniometer, and a z stage (15). Sample alignment was performed using a x-ray diode aligned to the primary x-ray beam following the same procedure as described elsewhere.<sup>15</sup> Upon measurements, the diode was removed from the beam path and the beamstop (3) was inserted, blocking the primary beam toward the 2D detector. The resulting 2D images were azimuthally integrated with Dioptas software.<sup>30</sup> Detector gaps, beamstop, and bad pixels were excluded from

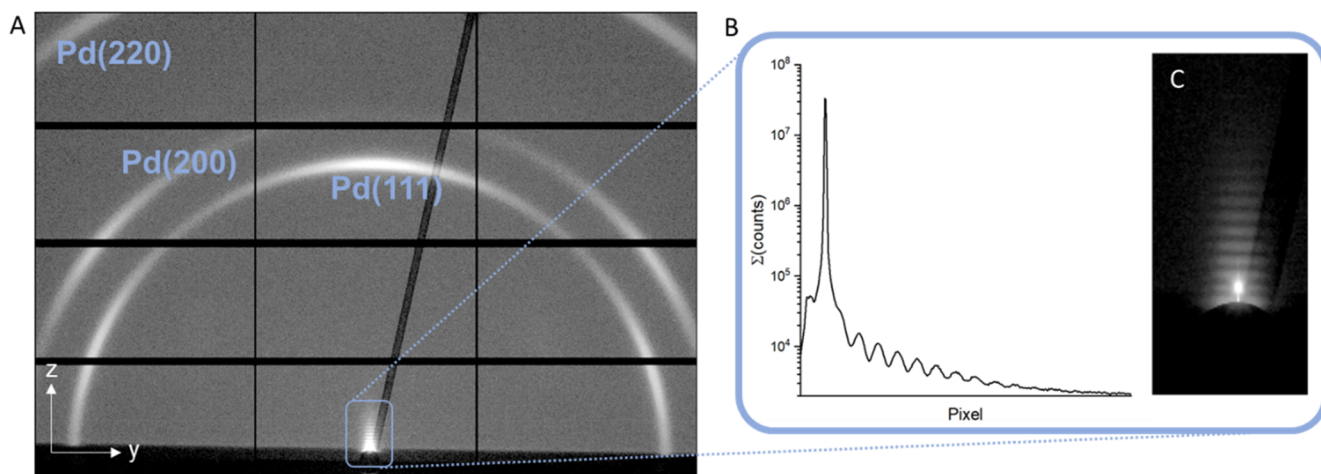


**FIG. 2.** Raw image of the x-ray measurement of the sputtered 3 nm Pd film on  $\text{SiO}_2$  on Si in ambient conditions [(a)-left] showing the Debye rings of the metal surface. An x-ray photon energy of 17 keV, an incidence angle of  $0.25^\circ$ , and an integration time of 280 s were applied. The (111), (200), and (220) intensities belong to the  $Fm\bar{3}m$  Pd (PDF 00-046-1043). A beamstop was used, blocking the primary x-ray beam. The right image (c) shows an enlarged section of the low angle region, revealing the Kiessig Fringes and the counts per pixel row (b).

the integration by applying an appropriate mask (Fig. S10). More elaborated protocols for data analysis are required for multi-layered thin films with texture, which include data correction for polarized light, the detector's solid angle,<sup>31</sup> correction of peak position due to refraction,<sup>32</sup> or sample misalignment,<sup>33</sup> and "missing wedges."<sup>34,35</sup>

## RESULTS AND DISCUSSION

For the evaluation of the cell Pt and Pd thin film samples were deposited in thicknesses between 3 and 20 nm on Si-wafers previously coated with an amorphous SiO<sub>2</sub> layer (see the description of samples and the deposition protocols in the supplementary material). Due to the positioning of the detector and use of a beamstop for the primary beam, angles below 0.8° are blocked. Since the 2D detector here is static in its vertical position, a maximum diffraction angle of 32° can be analyzed. An exemplary measurement of a 3 nm palladium film is shown in Fig. 2. Three Debye rings of a *Fm $\bar{3}m$*  Pd (PDF 00-046-1043) can be clearly observed (111, 200, and 220). The underlying PE-CVD grown SiO<sub>2</sub>, however, appears to be amorphous and elusive to this measurement, even though the estimated attenuation length of a 3 nm palladium film predicts it to be reachable by x rays (Fig. S11).<sup>36</sup> The thin film of Pd displays certain in-plane crystal orientation, highlighted by the difference in the intensity of the individual Debye rings in the  $\chi$  direction. Moreover, the Pd reflections are broad: to disentangle peak broadening due to (I) the optics of the setup, (II) the sample geometry

(GI nature of the experiment), and (III) the crystallite size, a standard and proper analysis must be performed (this is out of the scope of the current work). Besides the Debye rings, due to the use of a 2D detector, the Kiessig fringes can be observed. Although they are partially blocked by the beamstop, they could be analyzed providing simultaneous information on the roughness and thickness of the investigated sample. The bright spot in the fringes is the totally reflected x-ray beam.

In a first step, the contribution of the inner lid was studied. For this purpose, a 20 nm thick Pt-film on SiN<sub>x</sub> prepared by sputtering and PE-CVD, respectively, was measured (see the supplementary material for the details of the deposition). No diffraction is expected from this layer because the SiN<sub>x</sub> is amorphous, and the Pt film thickness of 20 nm is thicker than the x-ray attenuation length under these conditions (Fig. S11).<sup>36</sup> Figure 3 (top left) shows a comparison of the raw images obtained from the 2D detector. By closing the reactor with the lid, an additional Debye ring can be found in the very low angle region (around 2.8° at 17 keV), and a very broad halo is observed in the lower angle regions. These observations are in line with the grazing incidence scattering experiments on polyimide films.<sup>37</sup> Both features hardly interfere with the GIXRD measurements on thin metal films, which is why, next to their good chemical resistance and temperature stability, Kapton® and other polyimides are often chosen for these applications. Additionally, two small symmetric distinct Bragg spots can be seen at 19.2° and at around 7° (at 17 keV), which cannot be assigned to anything related to the

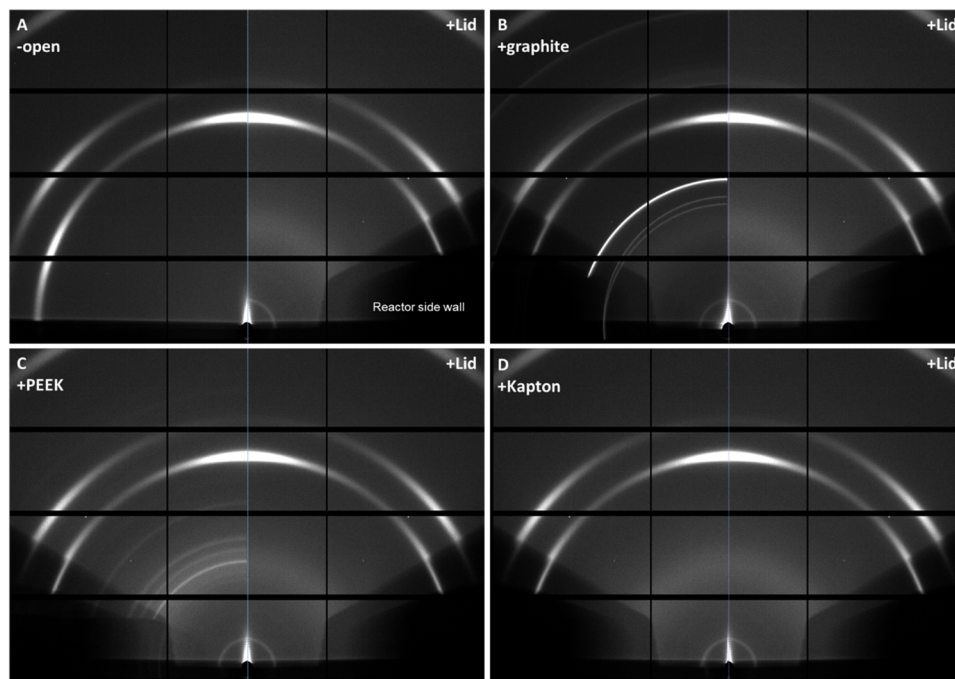


**FIG. 3.** Comparison of raw images of the x-ray measurements of a 20 nm Pt film on 20 nm SiN<sub>x</sub> on Si under ambient conditions (a) in the open; (b) with the graphite dome; (c) with the PEEK dome, and (d) with the Kapton® dome. For all the measurements, an x-ray photon energy of 17 keV, an incidence angle of 0.3°, and an integration time of 60 s were utilized. The left half of the image is obtained with the different domes, and the open cell is shown in comparison with the image obtained by just using the inner Kapton® lid. The right images are mirrored along the dashed line, allowing for a better direct comparison.



To confirm the cell's capabilities to perform *operando* measurements, acetylene hydrogenation was performed on the 3 nm Pd film at 150 °C applying a feed of 36.40 Nml/min H<sub>2</sub>, 1.21 Nml/min C<sub>2</sub>H<sub>2</sub>, and 7.88 Nml/min H<sub>2</sub> after a prior reduction in 80% hydrogen at 150 °C. The MS traces and detector images are shown in Fig. S9. A high conversion toward the products ethane and ethylene is indicated by the high intensities of the m/z 27 and 28 trace in comparison with that of the m/z 26 trace. At this point, a quantification of the reaction products and comparison to a designated catalytic reactor were unfortunately not possible. Therefore, although most probably capable of *operando* studies as well, at this point, only the *in situ* capabilities of this system can be proven. The interpretation of these measurements will be the subject of a separate publication.

## CONCLUSIONS AND OUTLOOK

An *in situ* cell for grazing-incidence diffraction and reflectivity measurements on films of a few nanometers for catalytic applications has been designed, constructed, and demonstrated. Its applicability to thin film characterization in a synchrotron environment has been demonstrated by time-resolved measurements of the phase transition of a 3 nm thick Pd film to Pd–H system. The high surface sensitivity at very low exposure times of 1 s demonstrates the applicability of the cell for thin films operating under highly dynamic processes. Since the background contribution of the Kapton® windows used here is negligible, there are no additional limitations to the nature of the analyzed samples when performing *in situ* GIXRD studies on nanocrystalline materials in this cell. In a synchrotron environment, the cell uniquely enables simultaneous GIXRD, XRR, and XRF measurements using the 2D detector, providing structural and textural information during *in situ* measurements and, most likely, also *operando* experiments. The materials chosen here currently limit the application to ambient pressures and temperatures up to 200 °C. However, the choice of windows facilitates the use of relatively low photon energies comparable to a laboratory Mo K $\alpha$  source. For use with a 0D detector, the current best performing Kapton® dome can be easily reshaped, allowing for the full 180° 2 $\Theta$  range with the current cell design. The design presented here already constitutes a very significant improvement to the state-of-the-art instrumentation and will be tested and further improved in a continuous effort to extend the limits for thin film based catalysts. By reducing the gas volume to a narrow slit, in contrast to commercial dome designs, dynamic experiments are now possible in this cell. More importantly, by excluding contact of thermocouples and heating wires to the gas phase, unwanted side reactions by the cell can be minimized, allowing a broader range of reactive gases to be used and paving the way for *operando* measurements under relevant conditions. To allow a broader range of applications in the future, the cell will be rebuilt using ceramics and glass, allowing higher temperatures and a more inert environment.

## SUPPLEMENTARY MATERIAL

The supplementary material contains Figs. S1–S10, providing additional information on the conducted experiments and the sample preparation.

## ACKNOWLEDGMENTS

The authors would like to thank Anupam Yadav, Martin Muske, Shivam, and Meysam Khodabakhshi for their help and support during the synchrotron experiments. The authors would like to gratefully acknowledge the staff at the BESSY II synchrotron in Berlin, Germany. The authors acknowledge the support from the Federal Ministry of Education and Research, Germany, in the framework of the project CatLab (Grant No. 03EW0015A).

## AUTHOR DECLARATIONS

### Conflict of Interest

The authors have no conflicts to disclose.

### Author Contributions

**Lukas Thum:** Conceptualization (equal); Formal analysis (equal); Investigation (equal); Methodology (equal); Visualization (lead); Writing – original draft (lead). **Manuela Arzmann:** Methodology (equal); Resources (equal); Visualization (supporting). **Ivo Zizak:** Data curation (equal); Methodology (equal); Resources (equal). **René Grüneberger:** Conceptualization (equal); Methodology (equal); Visualization (equal). **Alexander Steigert:** Methodology (equal); Resources (equal). **Nico Grimm:** Data curation (equal); Methodology (equal); Resources (equal). **Dirk Wallacher:** Conceptualization (equal); Resources (equal); Supervision (equal); Writing – review & editing (equal). **Rutger Schlatmann:** Funding acquisition (equal); Supervision (equal); Writing – review & editing (equal). **Daniel Amkreutz:** Funding acquisition (equal); Supervision (equal); Writing – review & editing (equal). **Albert Gili:** Conceptualization (equal); Formal analysis (equal); Investigation (equal); Project administration (lead); Visualization (equal); Writing – review & editing (lead).

## DATA AVAILABILITY

The data that support the findings of this study are available from the corresponding author upon reasonable request.

## REFERENCES

- H.-J. Freund, "Metal-supported ultrathin oxide film systems as designable catalysts and catalyst supports," *Surf. Sci.* **601**(6), 1438–1442 (2007).
- S. Kattel, P. J. Ramirez, J. G. Chen, J. A. Rodriguez, and P. Liu, "Active sites for CO<sub>2</sub> hydrogenation to methanol on Cu/ZnO catalysts," *Science* **355**(6331), 1296–1299 (2017).
- J. A. Rodriguez, S. Ma, P. Liu, J. Hrbek, J. Evans, and M. Pérez, "Activity of CeO<sub>x</sub> and TiO<sub>x</sub> nanoparticles grown on Au(111) in the water-gas shift reaction," *Science* **318**(5857), 1757–1760 (2007).
- S. W. Chee, T. Lunkenbein, R. Schlögl, and B. Roldán Cuenya, "Operando electron microscopy of catalysts: The missing cornerstone in heterogeneous catalysis research?," *Chem. Rev.* **123**(23), 13374–13418 (2023).
- B. B. Sarma, F. Maurer, D. E. Doronkin, and J. D. Grunwaldt, "Design of single-atom catalysts and tracking their fate using operando and advanced X-ray spectroscopic tools," *Chem. Rev.* **123**(1), 379–444 (2023).
- U. Hejral, M. Shipilin, J. Gustafson, A. Stierle, and E. Lundgren, "High energy surface X-ray diffraction applied to model catalyst surfaces at work," *J. Phys.: Condens. Matter* **33**(7), 073001 (2021).

- <sup>7</sup>A. Gili, L. Schlicker, M. F. Bekheet, O. Görke, D. Kober, U. Simon, P. Littlewood, R. Schomäcker, A. Doran, D. Gaissmaier, T. Jacob, S. Selve, and A. Gurlo, "Revealing the mechanism of multiwalled carbon nanotube growth on supported nickel nanoparticles by *in situ* synchrotron X-ray diffraction, density functional theory, and molecular dynamics simulations," *ACS Catal.* **9**(8), 6999–7011 (2019).
- <sup>8</sup>D. Teschner, J. Borsodi, A. Wootsch, Z. Révay, M. Hävecker, A. Knop-Gericke, S. D. Jackson, and R. Schlögl, "The roles of subsurface carbon and hydrogen in palladium-catalyzed alkyne hydrogenation," *Science* **320**(5872), 86–89 (2008).
- <sup>9</sup>Y. Niu, X. Huang, Y. Wang, M. Xu, J. Chen, S. Xu, M. G. Willinger, W. Zhang, M. Wei, and B. Zhang, "Manipulating interstitial carbon atoms in the nickel octahedral site for highly efficient hydrogenation of alkyne," *Nat. Commun.* **11**(1), 3324 (2020).
- <sup>10</sup>A. Gili, L. Schlicker, M. F. Bekheet, O. Görke, S. Penner, M. Grünbacher, T. Götsch, P. Littlewood, T. J. Marks, P. C. Stair, R. Schomäcker, A. Doran, S. Selve, U. Simon, and A. Gurlo, "Surface carbon as a reactive intermediate in dry reforming of methane to syngas on a 5% Ni/MnO catalyst," *ACS Catal.* **8**(9), 8739–8750 (2018).
- <sup>11</sup>R. Schlögl, "Heterogeneous catalysis," *Angew. Chem., Int. Ed.* **54**(11), 3465–3520 (2015).
- <sup>12</sup>L. Pandit, M.-A. Serrero, E. Saraç, A. Boubnov, and J.-D. Grunwaldt, "Versatile *in situ/operando* setup for studying catalysts by X-ray absorption spectroscopy under demanding and dynamic reaction conditions for energy storage and conversion," *Chem.–Methods* **2**(1), e202100078 (2022).
- <sup>13</sup>A. M. Beale, S. D. M. Jacques, E. K. Gibson, and M. Di Michiel, "Progress towards five dimensional diffraction imaging of functional materials under process conditions," *Coord. Chem. Rev.* **277–278**(May), 208–223 (2014).
- <sup>14</sup>B. Wollak, D. Espinoza, A. C. Dippel, M. Sturm, F. Vrljic, O. Gutowski, I. G. Nielsen, T. L. Sheppard, O. Korup, and R. Horn, "Catalytic reactor for operando spatially resolved structure–activity profiling using high-energy X-ray diffraction," *J. Synchrotron Radiat.* **30**(3), 571–581 (2023).
- <sup>15</sup>G. F. Harrington and J. Santiso, "Back-to-basics tutorial: X-ray diffraction of thin films," *J. Electroceram.* **47**(4), 141–163 (2021).
- <sup>16</sup>M. Farmand, A. T. Landers, J. C. Lin, J. T. Feaster, J. W. Beeman, Y. Ye, E. L. Clark, D. Higgins, J. Yano, R. C. Davis, A. Mehta, T. F. Jaramillo, C. Hahn, and W. S. Drisdell, "Electrochemical flow cell enabling: Operando probing of electrocatalyst surfaces by X-ray spectroscopy and diffraction," *Phys. Chem. Chem. Phys.* **21**(10), 5402–5408 (2019).
- <sup>17</sup>C. Örneke, A. Larsson, G. S. Harlow, F. Zhang, R. Kroll, F. Carlà, H. Hussain, U. Kivisäkk, D. L. Engelberg, E. Lundgren, and J. Pan, "Metastable precursor structures in hydrogen-infused super duplex stainless steel microstructure—An operando diffraction experiment," *Corros. Sci.* **176**(June), 109021 (2020).
- <sup>18</sup>D. Burkle, R. De Motte, W. Taleb, A. Kleppe, T. Comyn, S. M. Vargas, A. Neville, and R. Barker, "Development of an electrochemically integrated SR-GIXRD flow cell to study FeCO<sub>3</sub> formation kinetics," *Rev. Sci. Instrum.* **87**(10), 105125 (2016).
- <sup>19</sup>J. Gustafson, M. Shipilin, C. Zhang, A. Stierle, U. Hejral, U. Ruett, O. Gutowski, P.-A. Carlsson, M. Skoglundh, and E. Lundgren, "High-energy surface X-ray diffraction for fast surface structure determination," *Science* **343**(6172), 758–761 (2014).
- <sup>20</sup>S. Pfaff, J. Zhou, U. Hejral, J. Gustafson, M. Shipilin, S. Albertin, S. Blomberg, O. Gutowski, A. Dippel, E. Lundgren, and J. Zetterberg, "Combining high-energy X-ray diffraction with surface optical reflectance and planar laser induced fluorescence for *operando* catalyst surface characterization," *Rev. Sci. Instrum.* **90**(3), 033703 (2019).
- <sup>21</sup>D. C. A. Ivarsson, M. Neumann, A. A. Levin, T. Keilhauer, P. Wochner, and M. Armbrüster, "In operando GIXRD and XRR on polycrystalline In<sub>52</sub>Pd<sub>48</sub>," *Z. Anorg. Allg. Chem.* **640**(15), 3065–3069 (2014).
- <sup>22</sup>M. Nentwich, T. Weigel, C. Richter, H. Stöcker, E. Mehner, S. Jachalke, D. V. Novikov, M. Zschornak, and D. C. Meyer, "Sample chamber for synchrotron based *in-situ* X-ray diffraction experiments under electric fields and temperatures between 100 K and 1250 K," *J. Synchrotron Radiat.* **28**, 158–168 (2021).
- <sup>23</sup>A. P. Peter, K. Opsomer, C. Adelman, M. Schaekers, J. Meersschaert, O. Richard, I. Vaesen, A. Moussa, A. Franquet, T. Zsolt, and S. Van Elshocht, "Ulathrin NiGe films prepared via catalytic solid-vapor reaction of Ni with GeH<sub>4</sub>," *ACS Appl. Mater. Interfaces* **5**(19), 9605–9614 (2013).
- <sup>24</sup>M. C. Saint-Lager, A. Bailly, P. Dolle, R. Baudoing-Savois, P. Taunier, S. Garaudé, S. Cuccaro, S. Douillet, O. Geaymond, G. Perroux, O. Tissot, J. S. Micha, O. Ulrich, and F. Rieutord, "New reactor dedicated to in operando studies of model catalysts by means of surface X-ray diffraction and grazing incidence small angle X-ray scattering," *Rev. Sci. Instrum.* **78**(8), 083902 (2007).
- <sup>25</sup>R. Van Rijn, M. D. Ackermann, O. Balmes, T. Dufrane, A. Geluk, H. Gonzalez, H. Isern, E. De Kuyper, L. Petit, V. A. Sole, D. Wermeille, R. Felici, and J. W. M. Frenken, "Ultrahigh vacuum/high-pressure flow reactor for surface X-ray diffraction and grazing incidence small angle X-ray scattering studies close to conditions for industrial catalysis," *Rev. Sci. Instrum.* **81**(1), 014101 (2010).
- <sup>26</sup>R. Gleißner, E. E. Beck, S. Chung, G. D. L. Semione, N. Mukharamova, G. Gizer, C. Pistidda, D. Renner, H. Noei, V. Vonk, and A. Stierle, "Operando reaction cell for high energy surface sensitive X-ray diffraction and reflectometry," *Rev. Sci. Instrum.* **93**(7), 073902 (2022).
- <sup>27</sup>D. Bošković, "Reaktoren Für Spezielle Technisch-Chemische Prozesse: Mikrostrukturreaktoren," in *Handbuch Chemische Reaktoren* (Springer, Berlin, Heidelberg, 2019), pp. 1211–1246.
- <sup>28</sup>Helmholtz-Zentrum Berlin für Materialien und Energie, "MySpot: A versatile microfocussing station for scanning methods at BESSY II," *J. Large-Scale Res. Facil.* **2**, 1–10 (2016).
- <sup>29</sup>I. Zizak, "The MySpot beamline at BESSY II," *J. Large-Scale Res. Facil.* **2**, A102 (2016).
- <sup>30</sup>C. Prescher and V. B. Prakapenka, "DIOPTAS: A program for reduction of two-dimensional X-ray diffraction data and data exploration," *High Pressure Res.* **35**(3), 223–230 (2015).
- <sup>31</sup>Z. Jiang, "GIXSGUI: A MATLAB toolbox for grazing-incidence X-ray scattering data visualization and reduction, and indexing of buried three-dimensional periodic nanostructured films," *J. Appl. Crystallogr.* **48**, 917–926 (2015).
- <sup>32</sup>A. J. Pearson, "Structure formation and evolution in semiconductor films for perovskite and organic photovoltaics," *J. Mater. Res.* **32**(10), 1798–1824 (2017).
- <sup>33</sup>V. Holzer, B. Schrode, J. Simbrunner, S. Hofer, L. Barba, R. Resel, and O. Werzer, "Impact of sample misalignment on grazing incidence X-ray diffraction patterns and the resulting unit cell determination," *Rev. Sci. Instrum.* **93**(6), 063906 (2022).
- <sup>34</sup>L. E. Mundt and L. T. Schelhas, "Structural evolution during perovskite crystal formation and degradation: *In situ* and operando X-ray diffraction studies," *Adv. Energy Mater.* **10**(26), 1903074 (2020).
- <sup>35</sup>Y. Zhou, H. Zhou, J. Deng, W. Cha, and Z. Cai, "Decisive structural and functional characterization of halide perovskites with synchrotron," *Matter* **2**(2), 360–377 (2020).
- <sup>36</sup>See [https://henke.lbl.gov/optical\\_constants/atten2.html](https://henke.lbl.gov/optical_constants/atten2.html) for the estimation of the attenuation lengths of the x-rays at the applied photon energies and used materials.
- <sup>37</sup>B. J. Factor, T. P. Russell, and M. F. Toney, "Grazing incidence X-ray scattering studies of thin films of an aromatic polyimide," *Macromolecules* **26**(11), 2847–2859 (1993).
- <sup>38</sup>M. Doumeng, L. Makhlof, F. Berthet, O. Marsan, K. Delbé, J. Denape, and F. Chabert, "A comparative study of the crystallinity of polyetheretherketone by using density, DSC, XRD, and Raman spectroscopy techniques," *Polym. Test.* **93**(2020), 106878 (2021).
- <sup>39</sup>S. Dekura, H. Kobayashi, K. Kusada, and H. Kitagawa, "Hydrogen in palladium and storage properties of related nanomaterials: Size, shape, alloying, and metal-organic framework coating effects," *ChemPhysChem* **20**(10), 1158–1176 (2019).
- <sup>40</sup>M. Khanuja, B. R. Mehta, P. Agar, P. K. Kulriya, and D. K. Avasthi, "Hydrogen induced lattice expansion and crystallinity degradation in palladium nanoparticles: Effect of hydrogen concentration, pressure, and temperature," *J. Appl. Phys.* **106**(9), 093515 (2009).